Gating of Single-Layer Graphene with Single-Stranded Deoxyribonucleic Acids

*Jian Lin, Desalegne Teweldebrhan, Khalid Ashraf, Guanxiong Liu, Xiaoye Jing, Zhong Yan, Rong Li, Mihri Ozkan, Roger K. Lake, Alexander A. Balandin, and Cengiz S. Ozkan**

***P**atterning of biomolecules on graphene layers could provide new avenues to modulate their electrical properties for novel electronic devices. Single-stranded deoxyribonucleic acids (ssDNAs) are found to act as negative-potential gating agents that increase the hole density in single-layer graphene. Current–voltage measurements of the hybrid ssDNA/graphene system indicate a shift in the Dirac point and ''intrinsic'' conductance after ssDNA is patterned. The effect of ssDNA is to increase the hole density in the graphene layer, which is calculated to be on the order of 1.8×10^{12} cm^{-2}. This increased density is consistent with the Raman frequency shifts in the G-peak and 2D band positions and the corresponding changes in the G-peak full width at half maximum. Ab initio calculations using density functional theory rule out significant charge transfer or modification of the graphene band structure in the presence of ssDNA fragments.*

Keywords:
- density functional calculations
- DNA
- graphene
- patterning
- Raman spectroscopy

1. Introduction

Since its discovery in 2004,[1] graphene has emerged as a potential material for fabricating nanoelectronics beyond the complementary metal-oxide semiconductor (CMOS). With exceptionally high carrier mobility, electrically tunable conductance,[2] and very high thermal conductance,[3] graphene-based nanostructures have been employed in an increasing number of applications ranging from field-effect transistors[4–6] and gas sensors[7] to solar cells.[8] Because of the two-dimensional nanostructure and tunable surface chemistry, graphene layers are sensitive to the environment and chemical agents, which could provide ways to modulate their electrical properties through surface modification. To date, several different methods have been employed, including electrochemical modification[9] and chemical molecule decoration,[10–13] to modify the electrical properties of graphene layers. Deoxyribonucleic acid (DNA) and peptide nucleic acids (PNAs), which have base sequences that offer specificity, are attractive assembly linkers for bottom-up nanofabrication. Engineered single-stranded DNA (ssDNA) sequences are employed in the nanoarchitectures of end-functionalized single-walled carbon nanotubes (SWNTs) for device applications including resonant tunneling diodes, field-effect transistors, and biochemical sensors.[14–18] A thorough understanding of electrical transport through the interface between biological molecules such as DNA and graphene layers is still in its infancy.[19]

In this work, we investigated the modulation of carrier transport through graphene layers with overlaying ssDNA fragments via electrostatic interaction. We discovered that the role of ssDNA on the surface of graphene is analogous to applying a negative gate potential in conventional silicon CMOS architectures. Raman spectroscopy has been used in

[*] Prof. C. S. Ozkan, J. Lin
Department of Mechanical Engineering
University of California–Riverside
Riverside, CA 92521 (USA)
E-mail: cozkan@engr.ucr.edu
D. Teweldebrhan, K. Ashraf, G. Liu, X. Jing, Z. Yan, Prof. M. Ozkan, Prof. R. K. Lake, Prof. A. A. Balandin
Department of Electrical Engineering
University of California–Riverside
Riverside, CA 92521 (USA)
R. Li
Department of Biochemistry
University of California–Riverside
Riverside, CA 92521 (USA)

DOI: 10.1002/smll.200902379

small NANO MICRO

monitoring the doping of graphene layers.[20–22] We hypothesized that hole doping in graphene may induce a shift in both the G peak and the 2D band as well as a corresponding decrease in the full width at half maximum (FWHM) values. To validate the observation that the patterning of ssDNA on graphene layers induces an increased hole density, we further investigated the Raman spectra of graphene and the ssDNA/graphene hybrid system. We observed a well-defined shift in both the G peak and the 2D band after the graphene layer was patterned with ssDNA fragments. The absolute value of the observed shift correlates well with the current–voltage measurements and calculations for the induced carrier densities, which is in agreement with observations made where electron or hole doping was induced with an applied electric field.[20,21]

2. Results and Discussion

Single-layer graphene (SLG) flakes were selected with the help of micro-Raman spectroscopy using 2D band deconvolution and comparison of the intensities of the G peak and 2D bands.[23,24] This approach has proven to be reliable for identification of the number of layers in graphene flakes and for quality control. The absence of the disorder D band confirmed the high quality of the SLG used in this study, as shown in Figure 1.[25] Micro-Raman measurements were carried out in the backscattering geometry under 488 nm laser excitation.[23–26]

A statistical study based on atomic force microscopy (AFM) imaging of the SLG layer before and after ssDNA patterning is shown in Figure 2. The average thickness of the SLG layer increased from ≈1.0 to ≈1.8 nm, which indicated the formation of a thin layer of ssDNA on top of the SLG surface. From the AFM images, we observe the increased roughness of both the SiO_2 substrate and the SLG surface, which could be due to nonspecific and irregular binding of ssDNA fragments.

Current–voltage measurements on the SLG transistor were conducted in a vacuum (1.0×10^{-3} Torr) before and after ssDNA deposition to determine the modulation of the electrical characteristics. By employing a simple metal-oxide semiconductor field-effect transistor (MOSFET) model,[27] the carrier mobility was calculated using Equation (1):

$$\mu = \left(\frac{\Delta I_{ds}}{\Delta V_{gs}}\right) \Big/ \left(\frac{C_g W V_{ds}}{L}\right) \quad (1)$$

where I_{ds} and V_{ds} are the source–drain current and voltage, respectively, V_{gs} is the back-gate source voltage, L and W are the effective channel length and width, respectively, and C_g is the gate capacitance of the SLG device. Based on the data shown in Figure 3, the carrier mobility of the SLG transistor at room temperature before ssDNA patterning was calculated to be $\approx 1303\,cm^2\,(V\,s)^{-1}$, which is relatively lower than the reported values of about 2000 to $10^4\,cm^2\,(V\,s)^{-1}$ or even higher.[28,29] This low carrier mobility could be due to the contact resistance or surface impurities.[30,31] However, the mobility of this SLG is much higher than that of the biocomponents, and hence it is large enough for interfacing to the ssDNA molecules and enables the demonstration of tuning of the electrical properties of the SLG. From the two curves plotted, we deduce that the hole mobility of the SLG before and after ssDNA patterning is kept nearly constant.

Figure 3 shows the minimum conductance point (MCP, when the Fermi level is at the Dirac point) and the corresponding finite offset gate voltage, which depends on the charge impurity.[32] After ssDNA is patterned on the SLG devices, a parallel shift in the MCP is observed, which may originate from the creation of more charge impurities. In other words, when negatively charged ssDNA attaches to graphene, one needs to apply a more positive voltage to compensate for the additional charge.[33] The increase in the offset of the Dirac point gate voltage is around 25 V, and the conductance of the SLG transistor is also increased. Note that a control experiment was conducted in which a droplet of deionized water was placed on the SLG devices. After drying with a nitrogen flow, the current–voltage measurements under vacuum did not indicate any shift in the MCP.

The increased hole density induced by ssDNA patterning was calculated to be $3.45 \times 10^{12}\,cm^{-2}$ using the Drude model:

$$\Delta p = \left(R_2^{-1} - R_1^{-1}\right) \Big/ \left(\mu_p q \left(\frac{W}{L}\right)\right) \quad (2)$$

where R_2 and R_1 are the resistances of the SLG device before and after ssDNA patterning, respectively. This increase in the hole density was attributed to the following factor: ssDNA molecules with negative charge could act to induce a negative electric field effect (EFE) on the SLG.[19] This EFE could effectively induce the injection of extra holes in the graphene layer, hence the conductivity changes.

The change in the hole density is also calculated from a parallel-plate capacitor model based on the shift in the gate voltage of the MCP:

$$\Delta p = \frac{C_g}{q}\left(V_{MCP2} - V_{MCP1}\right) \quad (3)$$

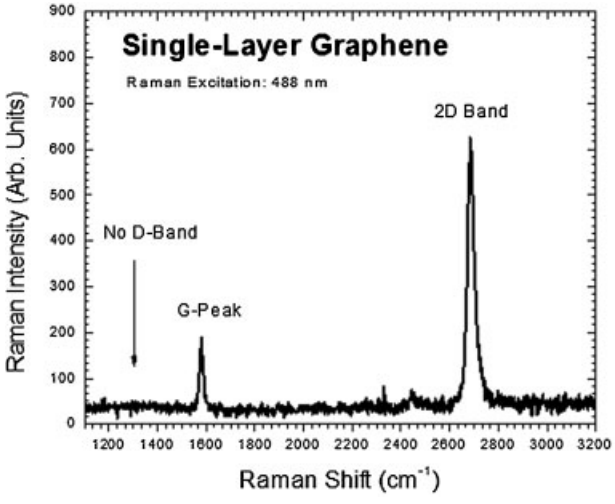

Figure 1. Raman spectrum collected from SLG between two contacts after device fabrication, which shows the typical features. The absence of the D band indicates that no substantial damage was caused during the fabrication process and electrical measurements.

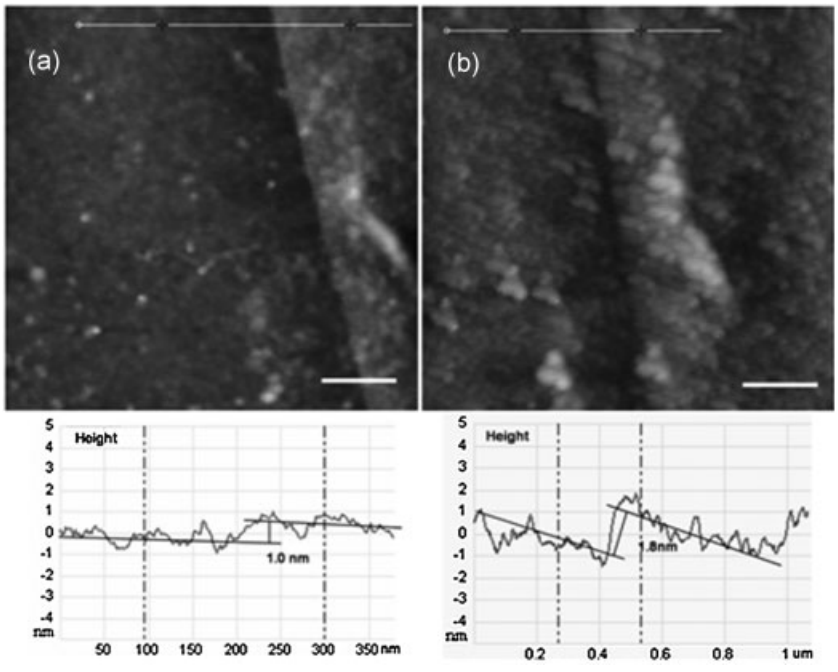

Figure 2. a,b) AFM images ($1.1 \times 1.1\ \mu m^2$, *Z*-range 15 nm) and corresponding cross-sectional profiles of SLG before (a) and after (b) patterning with ssDNA. The measured thickness of the SLG increases from ≈1.0 to ≈1.8 nm after ssDNA patterning. The increased roughness (shown below the images) is due to the nonspecific and irregular binding of ssDNA to the SLG. Scale bars: 200 nm; color bars:10 nm.

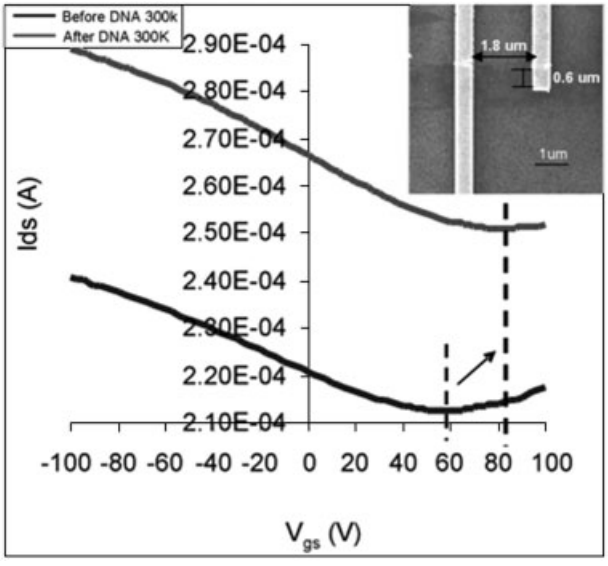

Figure 3. I_{ds}–V_{gs} characteristics of SLG before (black) and after (gray) ssDNA patterning of SLG devices at $T = 300$ K. The source–drain bias voltage is 100 mV. The dotted lines correspond to the Dirac point (minimum conductance point, MCP). The current–voltage measurements show that: 1) the gate voltage when the MCP is reached shifts from 60 to 80 V; and 2) the overall conductance shifts upwards. Inset: scanning electron microscopy image of the SLG device used in the measurements. The device channel length and effective width are 1.8 and 0.6 μm, respectively.

where V_{MCP2} and V_{MCP1} are the offset gate voltage in the MCP before and after ssDNA patterning, respectively. The excess hole density calculated from Equation (3) is $1.8 \times 10^{12}\ cm^{-2}$, which is comparable to the value calculated with the Drude model.

Raman spectroscopy has been intensively used for identifying the number of layers[34] and for monitoring the doping of graphene layers. The major Raman spectral features for graphene are the G band (optical phonon at long wavelengths) at ≈1584 cm^{-1} and the 2D band (associated with a two-phonon state) at ≈2700 cm^{-1} in pristine SLG. However, in doped graphene, the G-band and 2D-band frequencies as well as the FWHM value in the G peak are changed.[20–22,35,36]

To validate that ssDNA acting as a negative-potential gating agent on top of SLG can induce additional holes, we first measured the Raman spectrum on pristine SLG samples without device fabrication, which may induce some contaminants and residue on the surface.[37] Next, we patterned the same concentration of ssDNA on top of the SLG samples. Then the same Raman measurement was performed on the SLG samples with patterned ssDNA. A constant laser power below 2 mW was employed to ensure that the SLG flakes and the patterned ssDNA layer were not damaged and that local heating effects were ruled out.[3,38] Figure 4 shows the Raman spectra for which the main feature is the shift in the positions of the G band and the 2D band as well as their FWHM values. After ssDNA patterning, the average position of the G peak shifts from 1580 to 1582 cm^{-1}. According to measurements by Ferrari et al.,[20] a shift of ≈2 cm^{-1} corresponds to a hole concentration of approximately $2.0 \times 10^{12}\ cm^{-2}$, which is comparable to the value based on our electrical measurements. The reduction of the FWHM of the G peak after negative ssDNA gating is similar to the previously reported results for conventional electrostatic gating.[20–22,35,36] A detailed explanation for the decrease in the phonon G-peak FWHM value with an increase in carrier concentration has been previously provided.[20–22]

Apart from the interpretation of the G peak, the 2D peak originates from a second-order, double-resonant (DR) Raman scattering mechanism.[35] We measured the shift of the 2D peak position after ssDNA patterning. In our measurements, the 2D band line was averagely centered at 2685 cm^{-1} before ssDNA patterning and shifted to 2689 cm^{-1} after ssDNA patterning, which is in agreement with previously obtained results.[21,36] The observed decrease in the FWHM in the 2D band could be due to the fact that the electrostatic interaction between ssDNA and SLG could further modify the 2D band behavior. The behavior of the G peak shows that ssDNA fragments could provide a negative electric field gating effect on graphene layers. As a negative-potential gating agent, ssDNA fragments can modulate the Fermi level by inducing excess hole carriers. This shift of the Fermi level results in the expansion of the

small NANO MICRO

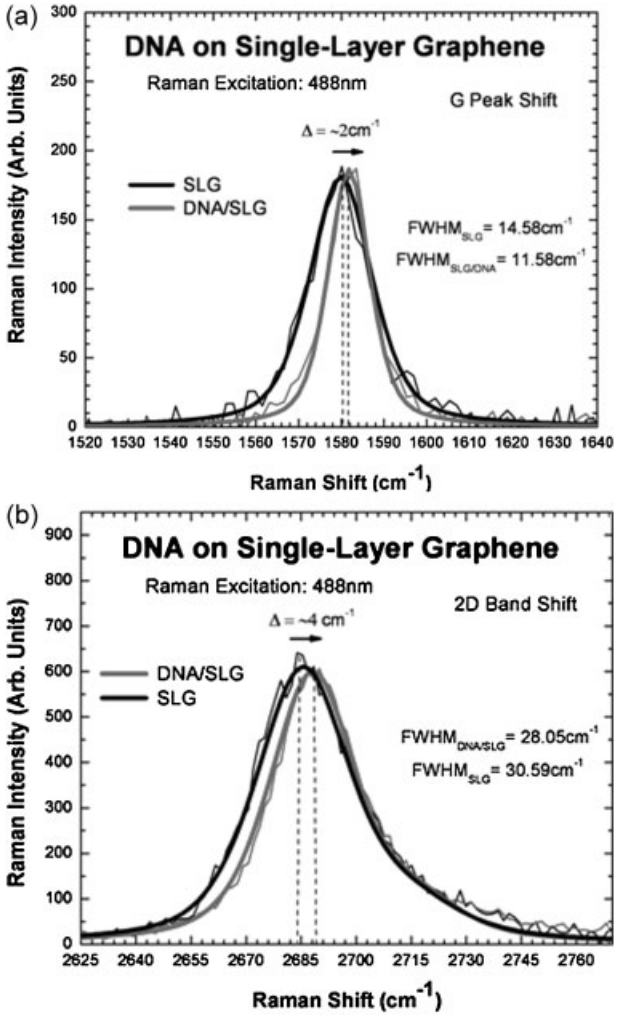

Figure 4. Micro-Raman spectroscopy of the signature G peak and the 2D band for pristine SLG and the ssDNA/SLG system. a) The G peak is centered at 1580 cm^{-1}, observed at an excitation wavelength of 488 nm, and shifts an average of 2 cm^{-1} after ssDNA patterning. b) The second-order 2D band shifts by $\approx$4 cm^{-1} as a result of ssDNA patterning. Both signature peaks also show relative shortening of their respective FWHM values.

equilibrium crystal lattice parameter with consequent stiffening of phonons and the onset of effects beyond the adiabatic Born–Oppenheimer approximation.[20,39]

The experimental data indicate that patterning of ssDNA causes an effective p-doping of the SLG. This could be the result of negative charges associated with ssDNA. However, there are two other hypotheses that could be investigated: 1) p-doping of the SLG could result from charge transfer between the SLG and the ssDNA; 2) the shift in the current versus gate-voltage curves could result from a modification of the SLG band structure due to an interaction with the ssDNA. To investigate these two possibilities, we performed ab initio density functional theory (DFT) calculations for adenine and guanine bases physisorbed on SLG. We focused on the bases since any charge transfer should occur in the frontier orbital, and the frontier orbital of ssDNA lies on its bases. Furthermore, any interaction that might modify the band structure of the SLG would most likely be mediated by the π orbitals of the bases interacting with the π orbitals of the SLG. This is analogous to the interaction of ssDNA bases with carbon nanotubes that has been observed; ssDNA has been found to wrap around SWNTs and form helices[16,17] with the bases physisorbing on the graphitic SWNT surface.[40]

The graphene supercell used in the calculations consists of 16 atomic layers in the zigzag direction and 12 atomic layers in the armchair direction. A single nucleoside is placed above the graphene sheet. Both adenine and guanine nucleosides were simulated. The initial structure of the base on the graphene layer was obtained following the results of Meng et al., where the structural properties of ssDNA physisorbed on SWNTs were determined by using directional optical absorbance and ab initio time-dependent DFT methods.[40] Calculations were performed using DFT implemented by the ab initio tight-binding molecular dynamics code FIREBALL.[41–43] The Becke–Lee–Yang–Parr (BLYP) exchange correlation functional is used with a double-numeric sp^3-localized orbital FIREBALL basis. In the self-consistent field calculation, a Fermi smearing temperature of 50 K and a self-consistent convergence factor of 10^{-5} are used. The two-dimensional Brillouin zone is sampled with six k-points in each direction during optimization. Structures are relaxed until all Cartesian forces on the atoms are <0.05 eV $Å^{-1}$.

The relaxed structure of SLG with the physisorbed adenine nucleoside is shown in Figure 5a. The distance between the SLG plane and the adenine base is approximately 3.35 Å. The calculated charge transfer from the SLG to adenine is 0.02 electrons, and the charge transfer from the SLG to guanine is 0.09 electrons. Both values are very small. This is expected from a consideration of the energy levels. The ionization potentials of adenine and guanine are 8.5 and 7.85 eV, respectively.[44] The electron affinities of adenine and guanine are of the order of 0.95 and 1.51 eV, respectively,[45] and the work function of SLG is 4.5 eV.[46] The occupied energy levels of the bases lie well below the Fermi level of SLG and the unoccupied levels are well above the Fermi level. Hence, the weak interaction through the π orbital should not cause charge transfer from SLG to the bases since the highest occupied molecular orbital (HOMO) levels are already filled. To achieve an effective hole doping of $\approx 2.0 \times 10^{12}$ cm^{-2}, and assuming an average charge transfer of 0.05 electrons per base, would require an areal density of base monomers of 4.0×10^{13} cm^{-2}. This value is more than an order of magnitude larger than the density that is estimated. Therefore, it is unlikely that this charge transfer is responsible for the apparent hole doping that is observed. The energy versus wave-vector relations for pristine SLG and for SLG with adenine nucleoside are shown in Figure 5b and c, respectively. The SLG band structure is unaffected by the adenine base. Most importantly, the band crossings at the Dirac point are left unchanged. Therefore, we cannot attribute the shift in the current versus gate-voltage curves to a change in the band structure of the SLG.

3. Conclusions

We have demonstrated that ssDNA fragments act as negative-potential gating agents resulting in an increase in the

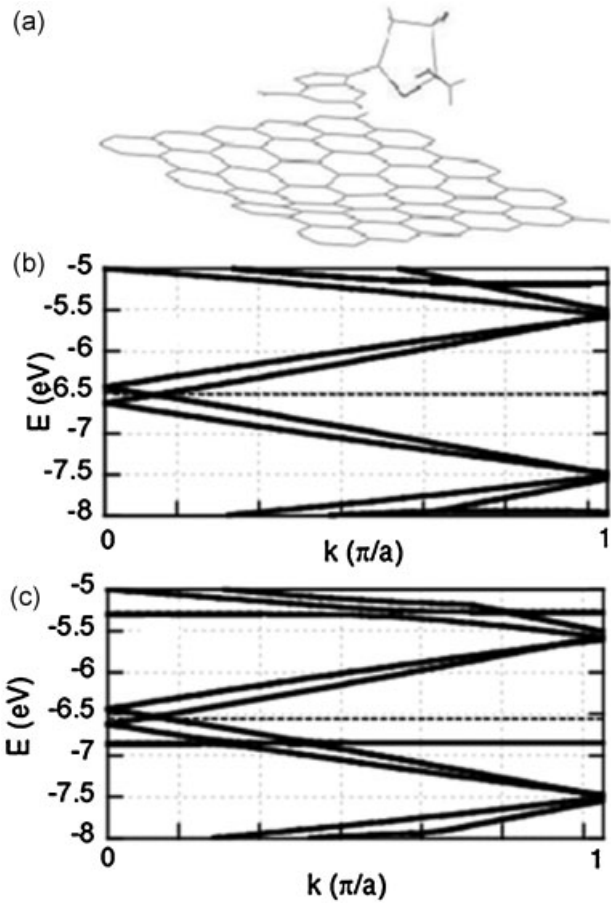

Figure 5. a) Adenine nucleoside on the graphene supercell. b) Energy versus *k* relation of a pristine graphene sheet along the armchair direction. A supercell is used for the repeat unit that contains 16 layers in the zigzag direction and 12 layers in the armchair direction. The dotted line shows the charge-neutral Fermi level of the system. c) Energy versus *k* relation of a graphene sheet with physisorbed adenine nucleoside. The dimensions of the graphene supercell are identical to those used in (b). The dotted line shows the charge-neutral Fermi level of the system.

hole density in graphene layers. By using current–voltage measurements, we computed an increase in the hole density with a value of about $1.8 \times 10^{12}\,cm^{-2}$ based on both the change in the resistance and the shift in the voltage of the MCP. This value is consistent with the peak-position shift of the G band and the 2D band of the Raman spectra. We ruled out changes due to charge transfer or modification of the SLG band structure due to the presence of ssDNA fragments. Furthermore, we discussed the relationships between the gating effect induced by the ssDNA fragments and the change in the phonon frequency, and demonstrated that patterning of biomolecules on graphene layers could provide new avenues to modulate their electrical properties.

4. Experimental Section

The graphene samples used in this study were extracted from highly oriented pyrolytic graphite (HOPG) slabs by mechanical exfoliation.[1,23,24,47] The graphene samples were deposited on p-type degenerately doped Si(100) wafers (p++) covered with 300-nm-thick thermally grown SiO_2. For device fabrication, source and drain contacts were patterned using electron-beam lithography followed by the deposition of source and drain metal consisting of 10-nm-thick Cr and 100-nm-thick Au layers (Temescal BJD-1800 electron-beam evaporator). To ensure that the graphene layer was intact after device fabrication, the samples were kept under vacuum until ready for analytical characterization.

The ssDNA sequence employed in this work was CGGGAGCTCAGCGGATAGGTGGGC. The engineered oligonucleotides (Sigma Genosys) were diluted in distilled water to obtain the stock solution. The concentration of the ssDNA solution was calculated to be $28.86\,mg\,mL^{-1}$. After the current–voltage ($I_{ds} - V_{gs}$) measurements of as-fabricated SLG transistors were obtained in a vacuum (1.0×10^{-3} Torr) at 300 K, a droplet (0.5 μL) of ssDNA solution was patterned over the active part of the device, followed by incubation for 30 min in the ambient environment and nitrogen drying. Then current–voltage measurements of SLG transistors with patterned ssDNA were conducted under vacuum (1.0×10^{-3} Torr) at 300 K.

Raman spectroscopy with a Renishaw instrument was used to identify the SLG as well as the Raman peak-position shift before and after patterning of ssDNA fragments on top of the SLG. The spectra were excited by a 488 nm visible-light laser. A Leica optical microscope with a 50× objective was used to collect the backscattered light from the graphene samples. The Rayleigh light was rejected by a holographic notch filter with a $160\,cm^{-1}$ cutoff frequency for 488 nm excitation. The spectra were recorded with an $1800\,lines\,mm^{-1}$ grating. A special precaution was taken to avoid local heating of the samples by the excitation laser. In order to achieve this, all measurements were carried out at a low excitation power, below 2 mW on the sample surface. The power density on the sample surface was verified with an Orion power meter. The spectral resolution of the instrument determined by the hardware was $\approx 1\,cm^{-1}$. The spectral resolution enhanced by software processing of the peak positions was below $0.5\,cm^{-1}$. The enhanced resolution of the instrument was sufficient to accurately resolve the shifts in peak positions under the conditions of the experiments through Lorentzian peak fitting. The spatial resolution was defined by the diffraction limit and estimated to be around 0.5 μm.

Acknowledgements

We gratefully acknowledge funding for this work by the FCRP-DARPA Center on Functional Engineered Nano Architectonics, The Riverside Public Utilities, an NSF-CMMI Award (0800680), the NSF-NSEC Center for Hierarchical Manufacturing-CHM (no. 0531171), and the NSF-MRSEC Center on Polymers (0213695).

[1] K. S. Novoselov, A. K. Geim, S. V. Morozov, D. Jiang, Y. Zhang, S. V. Dubonos, I. V. Grigorieva, A. A. Firsov, *Science* **2004**, *306*, 666.
[2] B. Huard, J. A. Sulpizio, N. Stander, K. Todd, B. Yang, D. Goldhaber-Gordon, *Phys. Rev. Lett.* **2007**, *98*, 236803.

[3] A. A. Balandin, S. Ghosh, W. Z. Bao, I. Calizo, D. Teweldebrhan, F. Miao, C. N. Lau, *Nano Lett.* **2008**, *8*, 902.
[4] G. Liu, J. Velasco, W. Z. Bao, C. N. Lau, *Appl. Phys. Lett.* **2008**, *92*, 203103.
[5] C. Stampfer, E. Schurtenberger, F. Molitor, J. Guttinger, T. Ihn, K. Ensslin, *Nano Lett.* **2008**, *8*, 2378.
[6] Z. H. Chen, Y. M. Lin, M. J. Rooks, P. Avouris, *Physica E (Amsterdam)* **2007**, *40*, 228.
[7] F. Schedin, A. K. Geim, S. V. Morozov, E. W. Hill, P. Blake, M. I. Katsnelson, K. S. Novoselov, *Nat. Mater.* **2007**, *6*, 652.
[8] Q. Liu, Z. F. Liu, X. Y. Zhang, N. Zhang, L. Y. Yang, S. G. Yin, Y. S. Chen, *Appl. Phys. Lett.* **2008**, *92*, 223303.
[9] R. S. Sundaram, C. Gomez-Navarro, K. Balasubranianian, M. Burghard, K. Kern, *Adv. Mater.* **2008**, *20*, 3050.
[10] D. C. Elias, R. R. Nair, T. M. G. Mohiuddin, S. V. Morozov, P. Blake, M. P. Halsall, A. C. Ferrari, D. W. Boukhvalov, M. I. Katsnelson, A. K. Geim, K. S. Novoselov, *Science* **2009**, *323*, 610.
[11] X. C. Dong, Y. M. Shi, Y. Zhao, D. M. Chen, J. Ye, Y. G. Yao, F. Gao, Z. H. Ni, T. Yu, Z. X. Shen, Y. X. Huang, P. Chen, L. J. Li, *Phys. Rev. Lett.* **2009**, *102*, 135501.
[12] W. Chen, S. Chen, D. C. Qi, X. Y. Gao, A. T. S. Wee, *J. Am. Chem. Soc.* **2007**, *129*, 10418.
[13] X. C. Dong, D. L. Fu, W. J. Fang, Y. M. Shi, P. Chen, L. J. Li, *Small* **2009**, *5*, 1422.
[14] Y. Xu, P. E. Pehrsson, L. W. Chen, R. Zhang, W. Zhao, *J. Phys. Chem. C* **2007**, *111*, 8638.
[15] R. R. Johnson, A. T. C. Johnson, M. L. Klein, *Nano Lett.* **2008**, *8*, 69.
[16] M. Zheng, A. Jagota, E. D. Semke, B. A. Diner, R. S. McLean, S. R. Lustig, R. E. Richardson, N. G. Tassi, *Nat. Mater.* **2003**, *2*, 338.
[17] M. Zheng, A. Jagota, M. S. Strano, A. P. Santos, P. Barone, S. G. Chou, B. A. Diner, M. S. Dresselhaus, R. S. McLean, G. B. Onoa, G. G. Samsonidze, E. D. Semke, M. Usrey, D. J. Walls, *Science* **2003**, *302*, 1545.
[18] X. Wang, F. Liu, G. T. S. Andavan, X. Y. Jing, K. Singh, V. R. Yazdanpanah, N. Bruque, R. R. Pandey, R. Lake, M. Ozkan, K. L. Wang, C. S. Ozkan, *Small* **2006**, *2*, 1356.
[19] N. Mohanty, V. Berry, *Nano Lett.* **2008**, *8*, 4469.
[20] S. Pisana, M. Lazzeri, C. Casiraghi, K. S. Novoselov, A. K. Geim, A. C. Ferrari, F. Mauri, *Nat. Mater.* **2007**, *6*, 198.
[21] A. Das, S. Pisana, B. Chakraborty, S. Piscanec, S. K. Saha, U. V. Waghmare, K. S. Novoselov, H. R. Krishnamurthy, A. K. Geim, A. C. Ferrari, A. K. Sood, *Nat. Nanotechnol.* **2008**, *3*, 210.
[22] J. Yan, Y. B. Zhang, P. Kim, A. Pinczuk, *Phys. Rev. Lett.* **2007**, *98*, 166802.
[23] I. Calizo, W. Z. Bao, F. Miao, C. N. Lau, A. A. Balandin, *Appl. Phys. Lett.* **2007**, *91*, 201904.
[24] I. Calizo, F. Miao, W. Bao, C. N. Lau, A. A. Balandin, *Appl. Phys. Lett.* **2007**, *91*, 071913.
[25] F. Parvizi, D. Teweldebrhan, S. Ghosh, I. Calizo, A. A. Balandin, H. Zhu, R. Abbaschian, *Micro Nano Lett.* **2008**, *3*, 29.
[26] D. Teweldebrhan, A. A. Balandin, *Appl. Phys. Lett.* **2009**, *94*, 013101.
[27] S. Adam, E. H. Hwang, V. M. Galitski, S. Das Sarma, *Proc. Natl. Acad. Sci. USA* **2007**, *104*, 18392.
[28] K. S. Novoselov, A. K. Geim, S. V. Morozov, D. Jiang, M. I. Katsnelson, I. V. Grigorieva, S. V. Dubonos, A. A. Firsov, *Nature* **2005**, *438*, 197.
[29] Y. B. Zhang, Y. W. Tan, H. L. Stormer, P. Kim, *Nature* **2005**, *438*, 201.
[30] V. Krstic, D. Obergfell, S. Hansel, G. L. J. A. Rikken, J. H. Blokland, M. S. Ferreira, S. Roth, *Nano Lett.* **2008**, *8*, 1700.
[31] J. H. Chen, C. Jang, S. Adam, M. S. Fuhrer, E. D. Williams, M. Ishigami, *Nat. Phys.* **2008**, *4*, 377.
[32] Y. W. Tan, Y. Zhang, K. Bolotin, Y. Zhao, S. Adam, E. H. Hwang, S. Das Sarma, H. L. Stormer, P. Kim, *Phys. Rev. Lett.* **2007**, *99*, 246803.
[33] A. B. Artyukhin, M. Stadermann, R. W. Friddle, P. Stroeve, O. Bakajin, A. Noy, *Nano Lett.* **2006**, *6*, 2080.
[34] A. C. Ferrari, J. C. Meyer, V. Scardaci, C. Casiraghi, M. Lazzeri, F. Mauri, S. Piscanec, D. Jiang, K. S. Novoselov, S. Roth, A. K. Geim, *Phys. Rev. Lett.* **2006**, *97*, 266407.
[35] C. Casiraghi, S. Pisana, K. S. Novoselov, A. K. Geim, A. C. Ferrari, *Appl. Phys. Lett.* **2007**, *91*, 233108.
[36] C. Stampfer, F. Molitor, D. Graf, K. Ensslin, A. Jungen, C. Hierold, L. Wirtz, *Appl. Phys. Lett.* **2007**, *91*, 241907.
[37] M. Ishigami, J. H. Chen, W. G. Cullen, M. S. Fuhrer, E. D. Williams, *Nano Lett.* **2007**, *7*, 1643.
[38] I. Calizo, A. A. Balandin, W. Bao, F. Miao, C. N. Lau, *Nano Lett.* **2007**, *7*, 2645.
[39] M. Lazzeri, F. Mauri, *Phys. Rev. Lett.* **2006**, *97*, 266407.
[40] S. Meng, W. L. Wang, P. Maragakis, E. Kaxiras, *Nano Lett.* **2007**, *7*, 2312.
[41] O. F. Sankey, D. J. Niklewski, *Phys. Rev. B* **1989**, *40*, 3979.
[42] J. P. Lewis, K. R. Glaesemann, G. A. Voth, J. Fritsch, A. A. Demkov, J. Ortega, O. F. Sankey, *Phys. Rev. B* **2001**, *64*, 195103.
[43] P. Jelinek, H. Wang, J. P. Lewis, O. F. Sankey, J. Ortega, *Phys. Rev. B* **2005**, *71*, 215101.
[44] *NIST Chemistry WebBook*, Vol. *69* (Eds: P. J Linstrom,, W. G. Mallard), **2008**, http://webbook.nist.gov.
[45] E. S. Chen, E. C. M. Chen, *Biochem. Biophys. Res. Commun.* **2001**, *289*, 421.
[46] G. Giovannetti, P. A. Khomyakov, G. Brocks, V. M. Karpan, J. van den Brink, P. J. Kelly, *Phys. Rev. Lett.* **2008**, *101*, 026803.
[47] K. S. Novoselov, D. Jiang, F. Schedin, T. J. Booth, V. V. Khotkevich, S. V. Morozov, A. K. Geim, *Proc. Natl. Acad. Sci. USA* **2005**, *102*, 10451.

Received: December 23, 2009

